AGU PUBLICATIONS

Paleoceanography

RESEARCH ARTICLE
10.1002/2016PA003063

Key Points:
- Middle to Late Pleistocene Mediterranean Outflow variability
- Precession paced glacial $\delta^{18}O$ enrichment events
- Shift in the sourcing of Mediterranean Outflow Water from Eastern to Western Mediterranean Sea at ~130 ka

Correspondence to:
S. Kaboth,
stefaniekaboth@ntu.edu.tw

Citation:
Kaboth, S., B. de Boer, A. Bahr, C. Zeeden, and L. J. Lourens (2017), Mediterranean Outflow Water dynamics during the past ~570 kyr: Regional and global implications, *Paleoceanography*, *32*, 634–647, doi:10.1002/2016PA003063.

Received 26 NOV 2016
Accepted 4 JUN 2017
Accepted article online 8 JUN 2017
Published online 22 JUN 2017

Mediterranean Outflow Water dynamics during the past ~570 kyr: Regional and global implications

Stefanie Kaboth[1,2], Bas de Boer[3], André Bahr[4], Christian Zeeden[5], and Lucas J. Lourens[2]

[1]Department of Geosciences, National Taiwan University, Taipei City, Taiwan, [2]Department of Earth Sciences, Faculty of Geosciences, Utrecht University, Utrecht, Netherlands, [3]Institute for Marine and Atmospheric research Utrecht, Utrecht University, Utrecht, Netherlands, [4]Institute of Earth Sciences, Ruprecht-Karls-Universität Heidelberg, Heidelberg, Germany, [5]Institute of celestial mechanics and ephemeris calculations, Observatoire de Paris, PSL Research University, Paris, France

Abstract The Gulf of Cadiz constitutes a prime area to study teleconnections between the North Atlantic Ocean and climate change in the Mediterranean realm. In particular, the highly saline Mediterranean Outflow Water (MOW) is an important modulator of the North Atlantic salt budget on intermediate water levels. However, our understanding of its paleoceanographic evolution is poorly constrained due to the lack of high-resolution proxy records that predate the last glacial cycle. Here we present the first continuous and high-resolution (~ 1 kyr) benthic $\delta^{18}O$ and $\delta^{13}C$ as well as grain size records from Integrated Ocean Drilling Program Site U1386 representing the last ~570 kyr. We find three distinct phases of MOW variability throughout the Late to Middle Pleistocene at Site U1386 associated with prominent shifts in its composition and flow strength. We attribute this long-term variability to changes in water mass sourcing of the MOW. Superimposed on the long-term change in water mass sourcing is the occurrence of distinct and precession paced $\delta^{18}O$ enrichment events, which contrast the pattern of global ice volume change as inferred from the global mean $\delta^{18}O$ signal (i.e., LR04) but mimics that of the adjacent Mediterranean Sea. We attribute these enrichment events to a profound temperature reduction and salinity increases of the MOW, aligning with similar changes in the Mediterranean source region. These events might further signify ice volume increases as inferred from significant sea level drops recorded in the Red Sea and/or increased influence of North Atlantic intermediate water masses when MOW influence was absent at Site U1386.

1. Introduction

The most striking hydrographic feature of the Gulf of Cadiz (Figure 1) is the Mediterranean Outflow Water (MOW) shaping the sedimentary depositional system along its upper (~500 water depth) and middle slope (~1000 m water depth) [*Baringer and Price*, 1997; *Borenäs et al.*, 2002; *Hernández-Molina et al.*, 2013]. The MOW constitutes of warm and relatively saline water masses exiting the Mediterranean Sea through the Strait of Gibraltar [*Ambar and Howe*, 1979; *Bryden et al.*, 1994; *Bryden and Stommel*, 1984]. As such, the Gulf of Cadiz is hydrographically directly linked to changes in the Mediterranean Sea source region through the MOW [*Bahr et al.*, 2015; *Jiménez-Espejo et al.*, 2015; *Kaboth et al.*, 2016; *Voelker et al.*, 2006]. The saline water masses of the MOW are thought to be an important modulator of the North Atlantic salt budget at intermediate water levels and proposed to precondition Atlantic Meridional Overturning Circulation (AMOC) [*Voelker et al.*, 2006].

Deciphering the interplay of MOW and the ambient North Atlantic intermediate water masses within the Gulf of Cadiz as well as their associated driving mechanisms over long geological time scales has so far presented a challenge to the scientific community due to the lack of long sedimentary records from the area predating the last climatic cycle [*Hernández-Molina et al.*, 2006; *Llave et al.*, 2006; *Rogerson et al.*, 2005; *Voelker et al.*, 2006]. Plio-/Pleistocene contourite drift sequences from the Gulf of Cadiz have been recently recovered during the IODP (Integrated Ocean Drilling Program) Expedition 339 [*Hernández-Molina et al.*, 2013; *Stow et al.*, 2013] allowing for a better understanding of the Gulf of Cadiz current system and climatic evolution.

Taking advantage of the unique hydrographic setting of the Gulf of Cadiz and its sensitivity to Mediterranean and North Atlantic climate variability, we aim to investigate the orbital scale variability of its intermediate water masses over the last five glacial-interglacial cycles (~570 kyr). For this, we have established the first benthic foraminifera $\delta^{18}O$ and $\delta^{13}C$ records of shallow marine (~560 m water depth) IODP Site U1386 located on the upper slope in the Gulf of Cadiz (see Figure 1). We compare our results to the benthic oxygen isotope

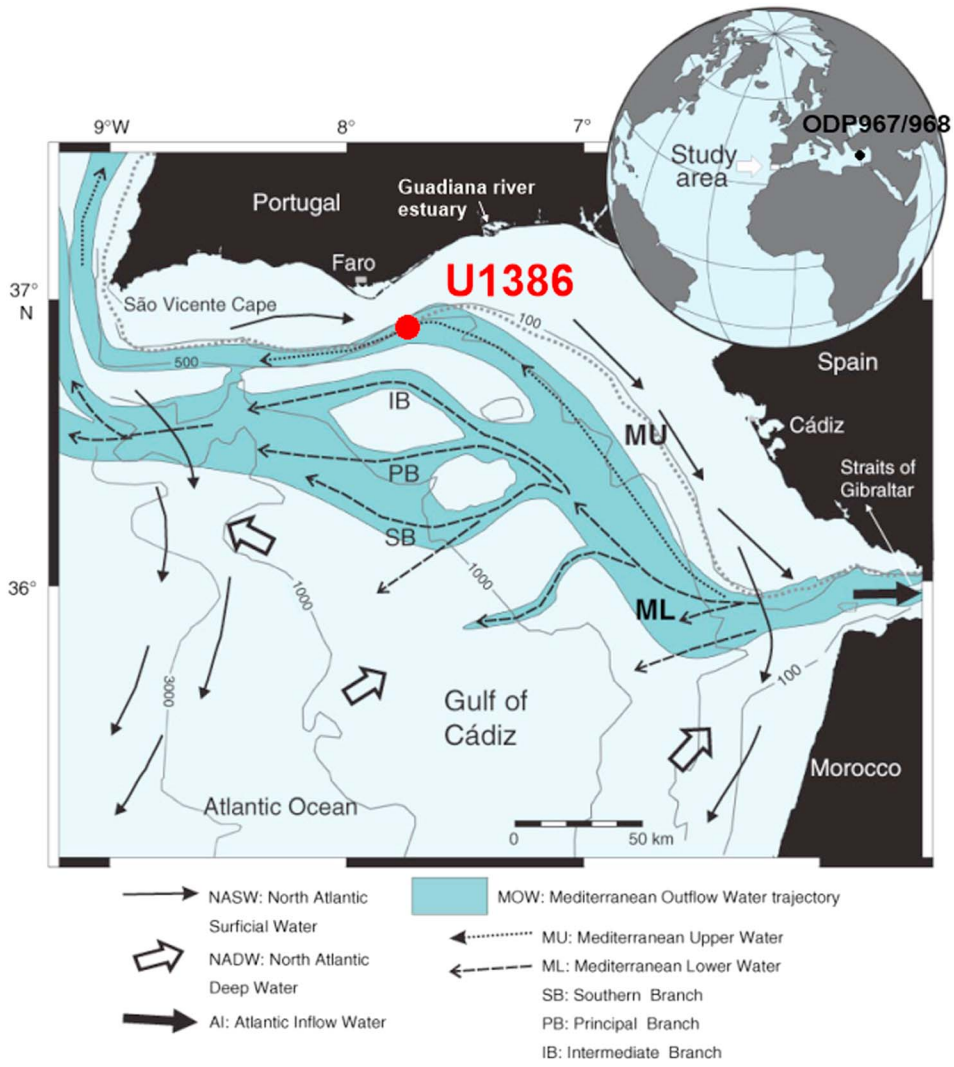

Figure 1. Study area; location map of the Gulf of Cadiz showing the recent flow pattern of MOW modified after [*Hernández-Molina et al.*, 2013; *Stow et al.*, 2013]. Site location of U1386 (upper MOW core, this study, red) and ODP967/968 in the Eastern Mediterranean Sea (black) is marked.

record of the ambient Mediterranean Sea, derived from the eastern basin [*Konijnendijk et al.*, 2015]. The results of this study demonstrate that the MOW underwent significant changes in both composition and flow dynamics during the Middle to Late Pleistocene which potentially impacted North Atlantic circulation patterns.

2. Modern Hydrography at Site U1386

The complex hydrography setting along the upper slope of the Gulf of Cadiz (Site U1386) is driven by the interplay of variable water masses (see Figure 2). At the bottom (>450 m) the hydrographic regime is dominated by northwestward migrating dense (>36 practical salinity unit (psu)) and warm (~13°C) upper branch of Mediterranean Outflow Waters [*Ambar and Howe*, 1979]. The MOW is predominately sourced of intermediate water masses from the Levantine basin in the Eastern Mediterranean Sea and changeable parts of Western Mediterranean Deep Water originating in the Gulf of Lions [*Millot*, 2014, 2009; *Millot et al.*, 2006].

Above the MOW, the intermediate and subsurface water column is influenced by subtropical water masses (14–16°C; ~36.2 psu) originating from the northern boundary of the eastern Azores Current branch that extends into the Gulf of Cadiz [*Peliz et al.*, 2009, 2005]. During spring and summer, colder and fresher

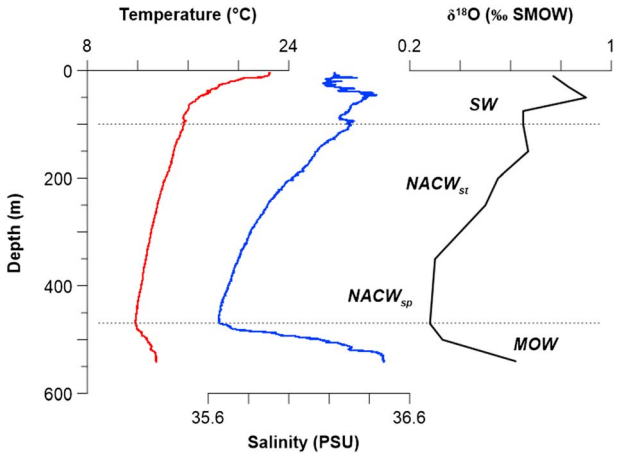

Figure 2. Modern Hydrography; CTD depth profile of temperature (red line), salinity (blue line), and $\delta^{18}O_{water}$ (black line) of EUROFLEETS-Iberian-Forams Cruise IB-F9 (36°48.40′N; 7°42.85′W) [*Voelker et al.,* 2015]. SW = surface water, $NACW_{st}$ = North Atlantic Central water of subtropical origin, $NACW_{sp}$ = North Atlantic water of subpolar origin, MOW = Mediterranean Outflow Water.

subsurface water masses can be traced along the upper slope region in the Gulf of Cadiz as identified by the salinity minimum above the MOW (see Figure 2). This process is linked to the seasonal upwelling systems along the Iberian Margin [*Fiúza et al.*, 1998]. With the relaxation of the upwelling (in the late fall to winter) the Iberian Poleward Current/Navidad Current establishes itself along the Iberian Margin associated with the northward bending of the subtropical front [*Peliz et al.*, 2005; *Stevenson*, 1977].

3. Materials and Methods

3.1. Site Location

Site U1386 was drilled during IODP Expedition 339 in November 2011 to January 2012 and is located southeast of the Portuguese Margin mounded on the Faro Drift along the Alvarez Cabral Moat at 36°49.68′N; 7°45.32′W in 561 m water depth (see Figure 1). The Faro drift is part of the Contourite Depositional System (CDS) of the Gulf of Cadiz [*Stow et al.*, 2013]. At recent, Site U1386 is directly influenced by the upper MOW flow core [*Baringer and Price*, 1997; *Borenäs et al.*, 2002; *Hernández-Molina et al.*, 2013]. The composite depth scale (meters composite depth, mcd) was developed from parallel holes at Site U1386 [*Hernández-Molina et al.*, 2013].

3.2. Stable Isotope Measurements and Interspecies Correlation

For this study, 658 sediment samples were analyzed for $\delta^{18}O$ at 30 cm intervals between 0 to 187.51 mcd (~570 kyr) resulting in an approximately 1 kyr resolution. The freeze-dried sediment samples were wet sieved into three fractions: (>150 μm, 150–63 μm and 63–38 μm; <38 μm fraction was discarded); residues were oven dried at 40°C. Stable oxygen isotope analyses were carried out on four to six specimens of the preferably epifaunal living foraminifera species *Planulina ariminensis* from the >150 μm size fraction. In the absence of *P. ariminensis* we selected specimen of the likewise preferably epifaunal living foraminifera *Cibicides ungerianus* [*Schönfeld*, 2002]. All selected specimens were crushed, sonicated in ethanol, and dried at 35°C. Stable isotope analyses were carried out on a CARBO-KIEL automated carbonate preparation device linked to a Thermo-Finnigan MAT 253 mass spectrometer at Utrecht University. The precision of the measurements is ±0.08‰ and ±0.03 for $\delta^{18}O$ and $\delta^{13}C$, respectively. The results were calibrated using the international standard NBS-19, and the in-house standard NAXOS. Isotopic values are reported in standard delta notation (δ) relative to the Vienna Pee Dee Belemnite (VPDB).

P. ariminensis was absent in 40 samples; resulting gaps were filled with *C. ungerianus*. The $\delta^{18}O$ values were corrected for interspecies induced isotopic offsets. The calculation of the interspecies isotopic offsets is based on 20 paired oxygen and carbon isotope measurements of both benthic species (Figure 3). The interspecies offsets were determined by applying a least squares linear regression equation. The Pearson correlation coefficient (R^2) between both species shows high correlation of 0.97 and 0.89 for $\delta^{18}O$ and $\delta^{13}C$, respectively. For $\delta^{18}O$ the calculated slope of linear relationship is ~1 with an intercept of −0.17‰ between *P. ariminensis* and *C. ungerianus* at Site U1386 which is slightly lower than the −0.3‰ isotopical shift in $\delta^{18}O$ reported by *Zahn et al.* [1987] between *P. ariminensis* and deeper infaunal *C. wuellerstorfi* from the Gulf of Cadiz. For $\delta^{13}C$ the calculated slope of linear relationship is ~0.5 with an intercept of ~1‰ between *P. ariminensis* and *C. ungerianus* at Site U1386 which is higher than the isotopical shift in $\delta^{13}C$ reported by *Zahn et al.* [1987] between *P. ariminensis* and deeper infaunal *C. wuellerstorfi* from the Gulf of Cadiz.

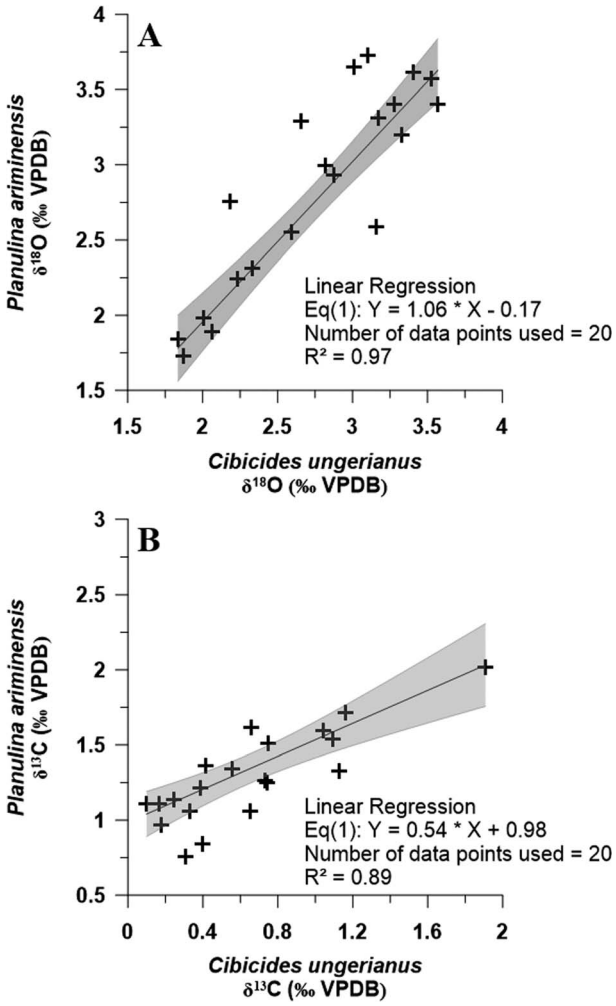

Figure 3. The (a) $\delta^{18}O$ and (b) $\delta^{13}C$ interspecies correlation between benthic foraminifera *Cibicides ungerianus* and *Planulina ariminensis* at Site U1386 for the Late and Middle Pleistocene. The correction is based on parallel measurements throughout the investigated interval. Linear square regression (black line) equation and Pearson correlation coefficient (R^2) are shown.

3.3. Grain Size

The oxygen isotope sample preparation was used to obtain weight percentages (wt %) of the grain size fractions >150 μm, 150–63 μm, 63–38 μm, and <38 μm for the investigated samples were obtained during sample preparation for isotope analyses. We concentrate on the grain size fraction between 150 and 63 μm which has been used previously as indicator for flow strength changes in the Gulf of Cadiz attributed to MOW variability [*Rogerson et al.*, 2005]. Even though untreated weight percentages hold a bias, it has been shown for the last climatic cycle that weight percentages mirror major peaks in Zr/Al records, considered a reliable recorder of MOW flow strength variability [*Bahr et al.*, 2014], and thus can be used to trace patterns of MOW variability [*Kaboth et al.*, 2016].

3.4. Mg/Ca Paleothermometry

For the Mg/Ca ratio measurements 11 samples were selected from Holocene and Last Glacial Maximum (LGM) as reference to the designated $\delta^{18}O$ enrichment events during marine oxygen isotope stage (MIS) 12 to MIS 6. From these samples five to seven specimen of *U. peregrina* from the >150 μm fraction (~250 μg) were gently crushed between two glass plates to open the chambers and then cleaned following the procedure of *Barker et al.* [2003]. The major steps of this method are (1) several water and ethanol washings to remove clay, (2) hydrogen peroxide treatment in a boiling water bath to eliminate organic matter, and (3) a short (30 s) dilute acid leaching with 0.001 *M* nitric acid to eliminate any adsorbed contaminants from test fragments. Prior to measurement, samples are dissolved in 350 ml of 0.075 *M* nitric acid, centrifuged to separate insoluble residues, and analyzed with a Varian Vista PRO simultaneous inductively coupled plasma atomic emission spectrometer at the Godwin Laboratory at Cambridge University. The Mg/Ca ratios were transferred into temperature estimates following *Cacho et al.* [2006]. This calibration is based on Western Mediterranean Deep Water top core samples and temperature adjusted to fit recent bottom water conditions in the region. We have applied this equation as other available transfer equations [e.g. *Bryan and Marchitto*, 2008; *Elderfield et al.*, 2012] produced unrealistic cold temperatures at Site U1386 during glacial periods of 1 to 3°C. This temperature offset potentially relates to the increased salinities of the MOW as Mg/Ca ratios often show a positive correlation to salinity [*Ferguson et al.*, 2008]. Additionally, we monitored in particular Mn and Fe element concentrations for the identification of potential contamination from clays or Mn-rich coatings. Long-term instrumental precision of the Mg/Ca ratio data, determined by replicate analyses of a standard solution, was ±0.33%. Uncertainty of the temperature estimates is based on parallel measurements and range between 0.15 to 1.2°C.

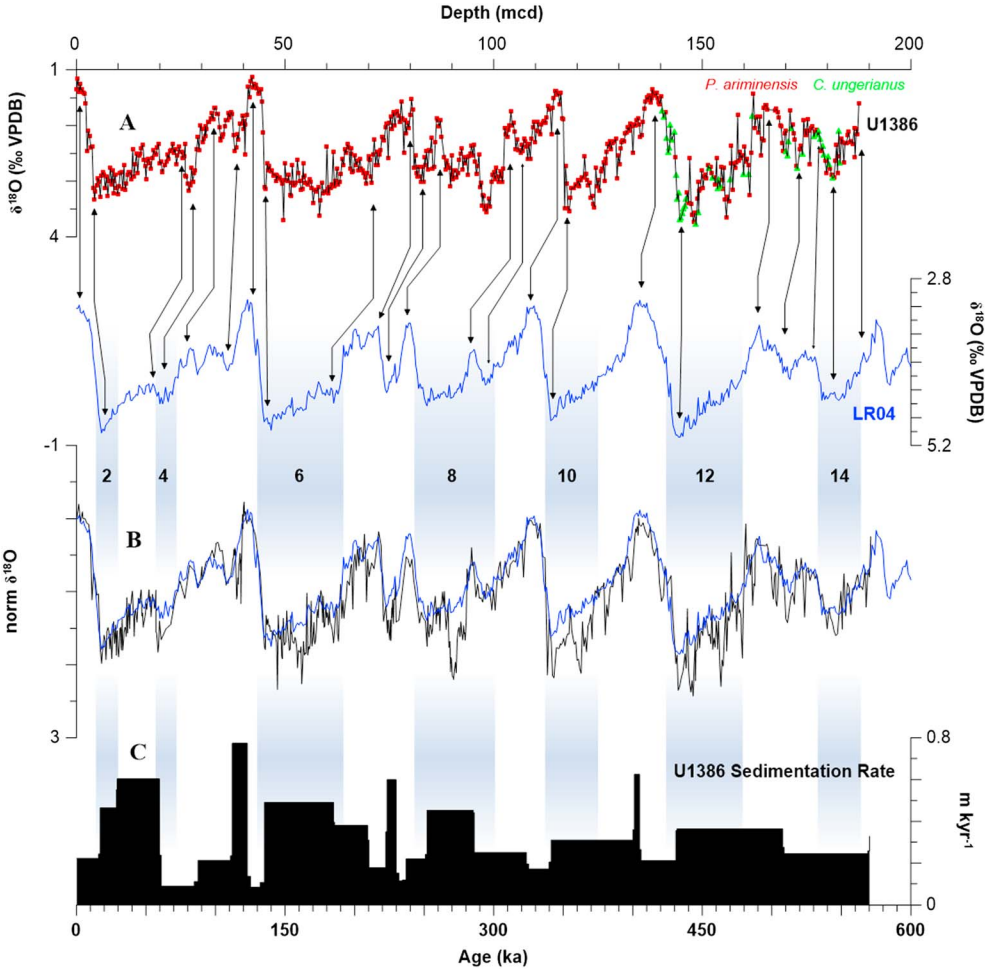

Figure 4. Chronology of Site U1386; blue columns represent MIS stages following [*Lisiecki and Raymo*, 2005]. (a) Correlation of δ^{18}O record on shipboard mcd scale correlated to the benthic δ^{18}O LR04 stack [*Lisiecki and Raymo*, 2005]. Lines with arrows indicate selected tie points used for the age model (a full list of tie points is available in Table 1). (b) Comparison of the normalized benthic δ^{18}O record of Site U1386 on the time scale according to our tuning, and normalized δ^{18}O LR04 stack on its age model [*Lisiecki and Raymo*, 2005]. (c) Sedimentation rate for Site U1386.

3.5. Chronology

The chronology is based on the visual correlation of the benthic δ^{18}O record at Site U1386 to the global mean benthic isotope stack LR04 [*Lisiecki and Raymo*, 2005] (see Figure 4a). To facilitate best correlation, we monitored the average sedimentation rate ~0.3 m/kyr [*Hernández-Molina et al.*, 2013; *Stow et al.*, 2013] of Site U1386 throughout the correlation process. The transitions T_I-T_V were used as initial tie points for the correlation. In addition, we utilized the maxima of the glacials and interglacials, respectively. The chronology of the MIS follows *Lisiecki and Raymo* [2005]. The applied correlation tie points are shown in Table 1.

3.6. Spectral Analysis

For the spectral analysis we applied the multitaper method as implemented in the "astrochron" R package [*Meyers*, 2014; *Rahim et al.*, 2014; *Thomson*, 1982]. The data were evenly spaced at 1 kyr resolution and linear detrended prior to analysis. Filtering was done using a taner filter [*Taner*, 1992] with cutoff frequencies at 0.029 and 0.075, and a roll-off rate of 10^3. Wavelets were determined using the "biwavelet" R package [*Gouhier et al.*, 2016; *R Core Team*, 2014] and follow methods described in *Grinsted et al.* [2004], *Liu et al.* [2007] and *Torrence and Compo* [1998].

Table 1. Age Calibration Points for the Visual Tuning of Benthic $\delta^{18}O$ Record of Site U1386 to the Global Mean Benthic $\delta^{18}O$ Stack of LR04 [*Lisiecki and Raymo*, 2005]

MCD	Age (ka)
0.0	0
2.0	9
4.0	18
9.1	29
27.8	60
30.2	87
35.5	112
44.0	123
45.0	135
69.5	185
79.0	210
81.3	223
85.5	230
86.3	237
89.6	252
105.0	286
114.5	324
117.4	341
136.0	401
138.5	405
144.0	431
172.0	508
187.2	570

3.7. Stable Oxygen Isotope Comparison Between Sites U1386 and ODP 967/968

To evaluate changes in Mediterranean Outflow influence at Site U1386 during the last ~570 kyr, we compared the $\delta^{18}O$ record from Site U1386 in the Gulf of Cadiz to the $\delta^{18}O$ stack of ODP Sites 967 and 968 in the eastern Mediterranean Sea [*Konijnendijk et al.*, 2015]. Due to the lack of sufficient long stable oxygen isotope records at intermediate water depth from the Mediterranean Sea during the Late to Middle Pleistocene, we are limited to the Eastern Mediterranean Sea deep-water record for comparison. Adjacent sites ODP 967 and 968 are located south of Cyprus near the Eratosthenes seamount at a water depth of 2554 m, and bath in Eastern Mediterranean Deep-Water (EMDW). Although EMDW is not directly contributing to MOW, it is interconnected due to convection and admixing to the overlying intermediate water masses, e.g., Levantine Intermediate Water (LIW) which is the predominant contributor to MOW [*Millot*, 2009; *Millot et al.*, 2006; *Rogerson et al.*, 2012]. The recorded isotopic signal at Sites ODP967/968 and, hence, EMDW functions therefore as a surrogate for long-term variability in the overlying LIW. The validity of this approach is supported by the fact that for the last ~130 kyr the $\delta^{18}O$ gradient between U1386 and ODP967/968 reproduces a similar pattern as observed between U1386 and the available LIW record at Site MD01-2472 [*Kaboth et al.*, 2016]. As an exception, our ODP967/968 might not be a good indicator for LIW properties during the formation of sapropels in the eastern Mediterranean Sea as those are a consequence of reduced intermediate and deep-water convection [*Cramp and O'Sullivan*, 1999; *Rossignol-Strick*, 1985].

For our comparison, we first corrected the two $\delta^{18}O$ records for interspecies offsets to equilibrium with the ambient water. The $\delta^{18}O$ stack at ODP Sites 967/968 is placed on a baseline of *Gyroidina altiformis* and *Gyroidina neosoldanii* [*Konijnendijk et al.*, 2015]. *Gyroidina* spp. is considered to calcify its $\delta^{18}O$ composition in equilibrium with the ambient water mass, therefore setting the baseline for our comparison [*Shackleton and Cita*, 1979]. Our oxygen isotope record of Site U1386 is placed on a *P. ariminensis* baseline with *C. ungerianus* values spliced in (see section 3.2). For the interspecies correction we followed the approach described in *Kaboth et al.* [2016]. As there are no direct correction values available for *P. ariminensis*, we followed *Zahn et al.* [1987] who showed a small offset of −0.3‰ for $\delta^{18}O$ between *P. ariminensis* and more often used *Cibicides wuellerstorfi*. To align Site U1386 to ODP 967/968, we adjusted the δ^{18O} values first to *C. wuellerstorfi* by −0.3‰ following *Zahn et al.* [1987] and second to equilibrium by adding 0.64‰ following [*Shackleton and Hall*, 1984].

4. Results

4.1. Chronology and Sedimentation Rate

The U1386 $\delta^{18}O$ record exhibits the major glacial-interglacial variability present in LR04 [*Lisiecki and Raymo*, 2005] over the past ~570 kyr (Figure 4b). The estimated mean sedimentation rate for Site U1386 (see Figure 4c) is ~0.4 m/kyr which differs from the relatively uniform sedimentation rate of ~0.25 m/kyr that has

been calculated from shipboard stratigraphy for the past 1.8 Myr [*Hernández-Molina et al.*, 2013; *Stow et al.*, 2013]. The resulting sedimentation rates vary between ~0.1 and ~0.8 m/kyr over the last ~570 kyr. With a sample spacing of approximately 0.3 m the resulting resolution of the composite benthic isotope record from Site U1386 is ~1 kyr. A doubling of the sedimentation rate coincides with the transition of MIS 12 to MIS 11 (~400 ka), MIS 8 to MIS 7 (~220 ka) and MIS 6 to MIS 5 (~125 ka). Three intervals exhibit relatively low sedimentation rates of $<$0.1 m/kyr: ~65 to 85 ka, ~132 ka, and ~230 ka.

4.2. Stable Oxygen and Carbon Isotopes

Figure 4b shows the comparison between the $\delta^{18}O$ record of Site U1386 normalized (by subtracting the respective most recent $\delta^{18}O$ value of the records) with the global mean $\delta^{18}O$ stack LR04 [*Lisiecki and Raymo*, 2005]. Evidently, IODP Site U1386 has been strongly influenced by global ice volume changes. This is made apparent by the good signal correlation of these records for the last ~570 kyr and highlights the ice volume-induced glacial-interglacial variability at Site U1386 (Figure 4b).

On glacial-interglacial timescales Site U1386 shows lightest values (~1.20–1.68‰) during interglacials MIS 5 and MIS 13 and glacial enrichment in $\delta^{18}O$ (~2.95–3.72‰) during MIS 14 and MIS 12. Terminations T_{IV} to T_I show depletions ranging between ~1.80‰ and ~2.19‰ (see Figure 4b).

While the $\delta^{18}O$ signal of Site U1386 and LR04 are coherently in-phase, diverging $\delta^{18}O$ values are visible especially during glacial periods (Figure 4b). These periods at Site U1386 are marked by a series of millennial-scale oscillations of triangular shape preceding the glacial maxima (see MIS 12, MIS 10, MIS 8, MIS 6, and partially MIS 4). These perturbations are of the order of up to ~1‰ (e.g., MIS 8) compared to the global mean $\delta^{18}O$. Similar $\delta^{18}O$ enrichment cannot be observed during MIS 2.

The $\delta^{13}C$ record at Site U1386 is shown in Figure 5a. Lightest values of $-$0.42‰ coincide with the transition MIS 10/MIS 9, and the heaviest values (~2.03‰) coincide with MIS 13. The $\delta^{13}C$ record shows a strong long-term trend starting from around ~475 kyr when a shift toward lighter $\delta^{13}C$ occurs compared to the older interval of the record (on average ~0.8‰). The trend is reversed around ~130 kyr when $\delta^{13}C$ values increase on average ~0.3‰.

4.3. Grain-Size

The mean grain size values (150–63 μm fraction) throughout the last ~570 kyr is ~2.5 wt %. Highest values of up to ~33 wt % are correlated with MIS 5 (Figure 5a). The grain size record shows glacial-interglacial variability with decreased values during glacial periods, and generally high-amplitude variations during interglacial periods. Interglacial grain size variability is, however, not uniform throughout the interglacial periods with highest values during MIS 5 and MIS 1 (~15 wt %) and lowest (~5% wt %) variations during MIS 11.

4.4. Mg/Ca Paleothermometry

The benthic Mg/Ca values range from on average 1.52 to 2.01 mmol/mol on glacial interglacial timescales. The resulting temperatures following *Cacho et al.* [2006] range from ~11°C during MIS 1 (interglacial conditions) to on average 8°C during the glacial periods of the last ~570 kyr (see Figure 5c).

5. Discussion

5.1. MOW Influence at Site U1386 During the Late to Middle Pleistocene

The grain size record at Site U1386 shows three distinct phases of MOW variability over the past 570 kyr. The last ~130 kyr (Phase I, see Figure 5a) have been already presented and discussed in *Kaboth et al.* [2016]. For this interval, strong MOW activity at Site U1386 was suggested during sea level high stands (MIS 5 and MIS 1) as indicated by high-amplitude grain size variability (Figure 4a). The largest grain size amplitude changes, indicating a strengthening of MOW flow at Site U1386, were shown to correlate to North Atlantic cold spells during the interglacial periods MIS 5 and MIS 1 [*Kaboth et al.*, 2016]. However, the authors also suggested the reduction or lack of MOW influence at Site U1386 during the full glacials MIS 4 and MIS 2 correlating with sea level low stands. These findings support previous suggestions of glacial MOW flowing deeper along the middle slope of the Gulf of Cadiz during the LGM [*Hernandez-Molina et al.*, 2014; *Llave et al.*, 2007; *Rogerson et al.*, 2005; *Schönfeld and Zahn*, 2000; *Voelker et al.*, 2006, 2009].

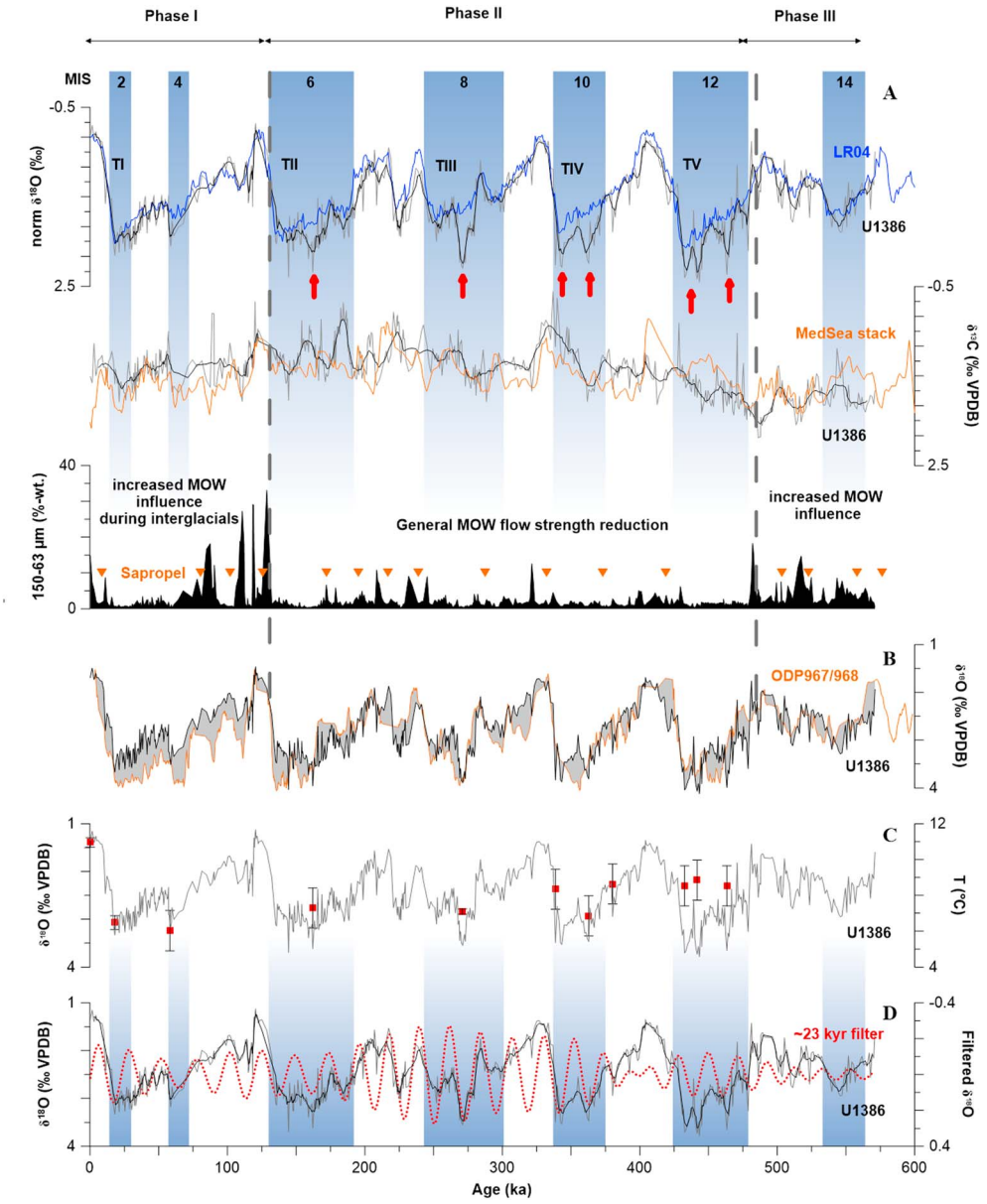

Figure 5. (a) Comparison of the normalized benthic $\delta^{18}O$ signal of Site U1386 (black line) and the global mean LR04 stack (blue line) [*Lisiecki and Raymo*, 2005], with the $\delta^{13}C$ record at Site U1386 (black) and the MedSea $\delta^{13}C$ stack (orange line [*Wang et al.*, 2010]), and the grain size (150–63 µm fraction) at Site U1386. The glacial $\delta^{18}O$ enrichment events are marked by small red arrows. MIS stages (blue columns) follow [*Lisiecki and Raymo*, 2005] (b) Comparison of the interspecies corrected $\delta^{18}O$ signals between Site U1386 (black line) and ODP sites 967 and 968 (orange line) [*Konijnendijk et al.*, 2015]. Isotopic gradient marked as grey shaded area. (c) *U. peregrina* Mg/Ca-based mean temperature estimates (red crosses) for the glacial $\delta^{18}O$ enrichment events relative to the recent at Site U1386. For visual reference the benthic $\delta^{18}O$ record (grey line) at Site U1386 is also given. (d) The ~23 kyr filter (red dotted line) of the benthic $\delta^{18}O$ signal superimposed on the stable oxygen isotope signal at Site U1386.

Accordingly, the strongly decreased grain size variability in Phase II between ~475 kyr (MIS 13/MIS 12) and ~130 kyr (MIS 6/MIS 5) would suggest that MOW influence at Site U1386 was genuinely reduced or absent prior to the upper Pleistocene during both glacial and interglacial periods (Figure 5a). The comparison between the $\delta^{18}O$ records of Site U1386 and that of ODP Sites 967/968 in the Eastern Mediterranean Sea [*Konijnendijk et al.*, 2015], however, point to a different scenario (Figure 5b). This comparison yields a persistent isotopic gradient during the past ~130 ka [*Kaboth et al.*, 2016] and a strongly reduced gradient, both

during glacial and interglacial periods, prior to 130 ka. The absence of a similar distinct gradient between 130 and 570 kyr suggests a permanent MOW influence at Site U1386. Evidently, this MOW influence must have largely ceased during the glacial periods of the last climatic cycle. As grain size variability is a proxy for MOW flow speed and in extension its density rather than its presence, the lack of profound grain size variability during Phase II might be explained by a shift in the major source regions (i.e., western versus eastern Mediterranean Sea basins) of MOW. The convergence of the $\delta^{18}O$ records from Site U1386 with those of the Eastern Mediterranean Sites 967/968 during Phase II implies that MOW was predominantly composed of LIW. A less dense MOW would tentatively be associated with decreased sediment interaction and hence suppressed flow strength as evidenced by the reduced grain size variability during Phase II. However, it has been argued that the internal structure of the ambient North Atlantic intermediate water column is the most prominent driver of MOW flow behavior on glacial-interglacial timescales [*Rogerson et al.*, 2012]. As the reduction of flow strength at Site U1386 during Phase II is a general phenomenon and not directly linked to glacial-interglacial climate change, it seems more likely that changes within the Mediterranean source region could have been the driving mechanisms behind the difference between Phase I and II. In this light, significant portions of denser Western Mediterranean Deep Water (WMDW) might have played a greater role during the entire Phase I as has been already suggested for the LGM [*Voelker et al.*, 2006]. A denser MOW during Phase I fed more dominantly into the lower MOW core at greater depth along the middle slope on the expense of the upper MOW core at Site U1386 aligning with the increased isotopic gradient between Site U1386 and ODP 967/968 (Figure 5b). Additionally, a renewed tectonic activity from ~600 kyr to ~300 kyr [*Hernanndez-Molina et al.*, 2015] could have caused a modification of the MOW pathway along the upper slope and a reduction in MOW flow strength resulting in a general fining of the sediment. Site U1386 is also closely located to the moat generated by the MOW [*Hernández-Molina et al.*, 2013; *Stow et al.*, 2013] making it most sensitive to variations in bottom current velocity as it represents the upper boundary layer of the MOW [*Bahr et al.*, 2015]. Nevertheless, the presence of at least short-term, interglacial MOW variability can be traced in the grain size changes at Site U1386 during MIS 11, MIS 9, and MIS 7 (Figure 5a).

For the oldest interval (Phase III) between ~570 ka and ~475 ka the high grain size amplitude changes, similar to those of the last climatic cycle, point again to a stronger MOW flow strength at Site U1386 at the end of the Middle Pleistocene transition (Figure 5(a)). A pronounced oxygen isotopic gradient between Site U1386 and ODP 967/968, as found for Phase I, did not occur during the glacial period of MIS 14 (Figure 5b), indicating that MOW influence remain present at Site U1386 during Phase III. This interpretation is supported by the increased variability found in the grain size record. Most likely, the less severe climate conditions and associated higher sea level stands during MIS 14 compared to MIS 2 and MIS 4 did not lead to a significant reduction in MOW flow speed along Site U1386.

To gain further insight into possible changes of the MOW source region during the last 570 kyr, we utilized our $\delta^{13}C$ record at Site U1386. The results, at first glance, also suggest a three-phased behavior, in line with our grain size record (Figure 5a), that could provide further evidence for substantial changes in the composition of the MOW as the driving mechanism behind the observed grain size variability. Yet the superimposed long-term trend has been recognized globally [*Wang et al.*, 2003] as well as in the surface water signal of the Mediterranean Sea [*Wang et al.*, 2010] and has been attributed to profound changes in the global carbon reservoir (e.g., Middle Brunhes event at ~430 ka) [*Wang et al.*, 2003]. A direct comparison between our $\delta^{13}C$ signal at Site U1386 and the Mediterranean Sea is not possible due to the lack of long-term benthic records. The close similarities in phasing and amplitude between the planktic, eastern Mediterranean Sea and Site U1386 $\delta^{13}C$ records (Figure 5(a)) nonetheless support the suggestion that water masses at Site U1386 were dominantly of Mediterranean origin throughout the last 570 kyr. A substantial and long-lasting switch from MOW to ambient North Atlantic intermediate water masses with relative light $\delta^{13}C$ values [*Voelker et al.*, 2006] would most probably have resulted in a distinct offset between both $\delta^{13}C$ records.

5.2. Glacial $\delta^{18}O$ Enrichment Events at Site U1386 and Their Relation to Precession

The $\delta^{18}O$ record of Site U1386 reveals prominent enrichments (up to ~1‰, e.g., MIS 8, Figure 5a) during the full glacial periods between MIS 12 and MIS 6 and the transitional climate conditions (MIS 13/MIS 12 and MIS 11/MIS 10), i.e., the time period encompassing the shift in water mass composition at Site U1386 between ~470 and 130 ka, that are clearly absent in the LR04 global stack (Figure 5a). The power spectrum

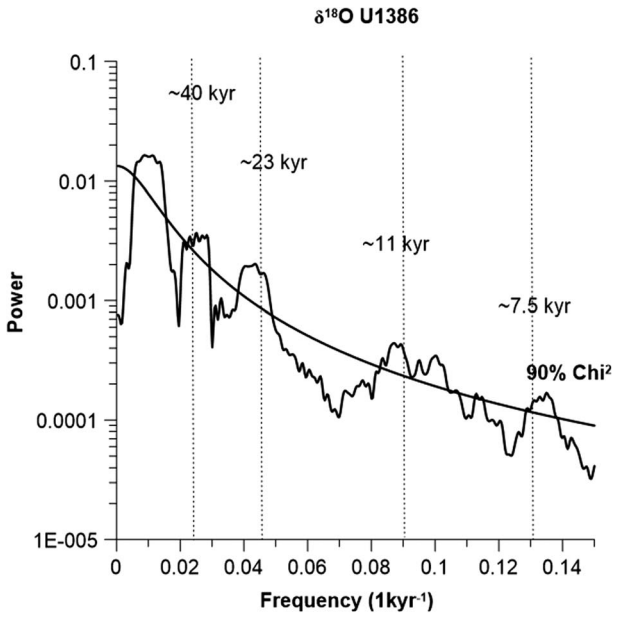

Figure 6. Power spectrum of $\delta^{18}O$ record of Site U1386 with 90% confidence interval (black line). The main frequency of obliquity (~40 kyr), precession (~23 kyr), semiprecession (~11 kyr), and a third precession (~7.5 kyr) is marked.

(Figure 6) and filtered ~23 kyr signal both give strong indication that these observed strong glacial $\delta^{18}O$ enrichment events are related to precession variability (Figure 5d).

The comparison between Site U1386 and the Mediterranean Sea (Figure 5b) might provide the most straightforward explanation for these precession-related enrichment events as glacial enrichment events similar in amplitude can also be found in the eastern Mediterranean Sea [*Konijnendijk et al.*, 2015]. It was suggested that these perturbations (e.g., within MIS 8) reflect a sea level drawdown and associated temperature drop in extension to major ice volume advances as similar excursions were also identified in the Red Sea sea level reconstructions [*Grant et al.*, 2014; *Rohling et al.*, 2009; *Siddall*, 2004]. If the $\delta^{18}O$ enrichment events at Site U1386 coincide with MOW influence, it seems feasible that the Mediterranean sea level signal was eventually transported to Site U1386. This suggests that the $\delta^{18}O$ enrichment events might, in fact, represent an imprint of ice volume-related changes that are not depicted in the global mean stack. A fraction of the glacial $\delta^{18}O$ enrichment events at Site U1386 might also derive directly from MOW influence which could also explain their apparent precession pacing as a distinct precession-related signal was found for MOW production during the past 150 kyr [*Bahr et al.*, 2015]. In particular, during times of (predominantly) precession-driven sapropel formation in the eastern Mediterranean, MOW was reduced, causing a decline of the flow speed within the major branches of MOW in the Gulf of Cadiz. Hence, besides a possible glacioeustatic forcing mechanism, these $\delta^{18}O$ enrichment events could also reflect a direct response to insolation driven hydrographic changes in the Mediterranean source area [*Bahr et al.*, 2015; *Kaboth et al.*, 2016]. Such a scenario is in accordance with climate modeling experiments showing that MOW is generally increased during precession maxima when dryer and colder climate background conditions prevailed over the Mediterranean region [*Bosmans et al.*, 2014]. This aligns with our findings as the strongest $\delta^{18}O$ enrichment events throughout the Late Pleistocene (e.g., MIS 8 and MIS 6) exclusively coincide with precession maxima. Furthermore, the wavelet analysis visualizes that the precession forcing of $\delta^{18}O$ enrichment at Site U1386 is more prominent during glacial stages similar to Sites ODP 967/968 and contrasting the precession contribution to ice volume change which is more dominant during transitional and early interglacial periods (see Figure 7). This might also be seen as an indication that the origin of these $\delta^{18}O$ enrichment events is of a more regional rather than global character.

Our bottom water temperature estimates of ~6–8°C based on benthic Mg/Ca measurements for the enrichment events at Site U1386 are similar to that of the LGM (Figure 5c). This indicates that bottom water temperatures dropped on glacial-interglacial timescales by ~3 to 5°C, i.e., in accordance with the global mean [*Köhler et al.*, 2010]. It becomes apparent that the glacial-induced temperature decrease did substantially contribute to the increase of $\delta^{18}O$ during the glacial periods but provide no indication that a more profound cooling occurred during the peaks of the $\delta^{18}O$ enrichment events relative to the LGM conditions at Site U1386. As a similar decrease in temperature is also expected for the Mediterranean Sea, it seems possible that our bottom water temperature estimates might represent glacial MOW properties. The rather steady temperature decrease between the peaks of the $\delta^{18}O$ enrichment events during, e.g., MIS 8 and MIS 6 compared to the LGM also stands in contrast to the glacial depiction of the LR04 where MIS 8 and MIS 6 are not just

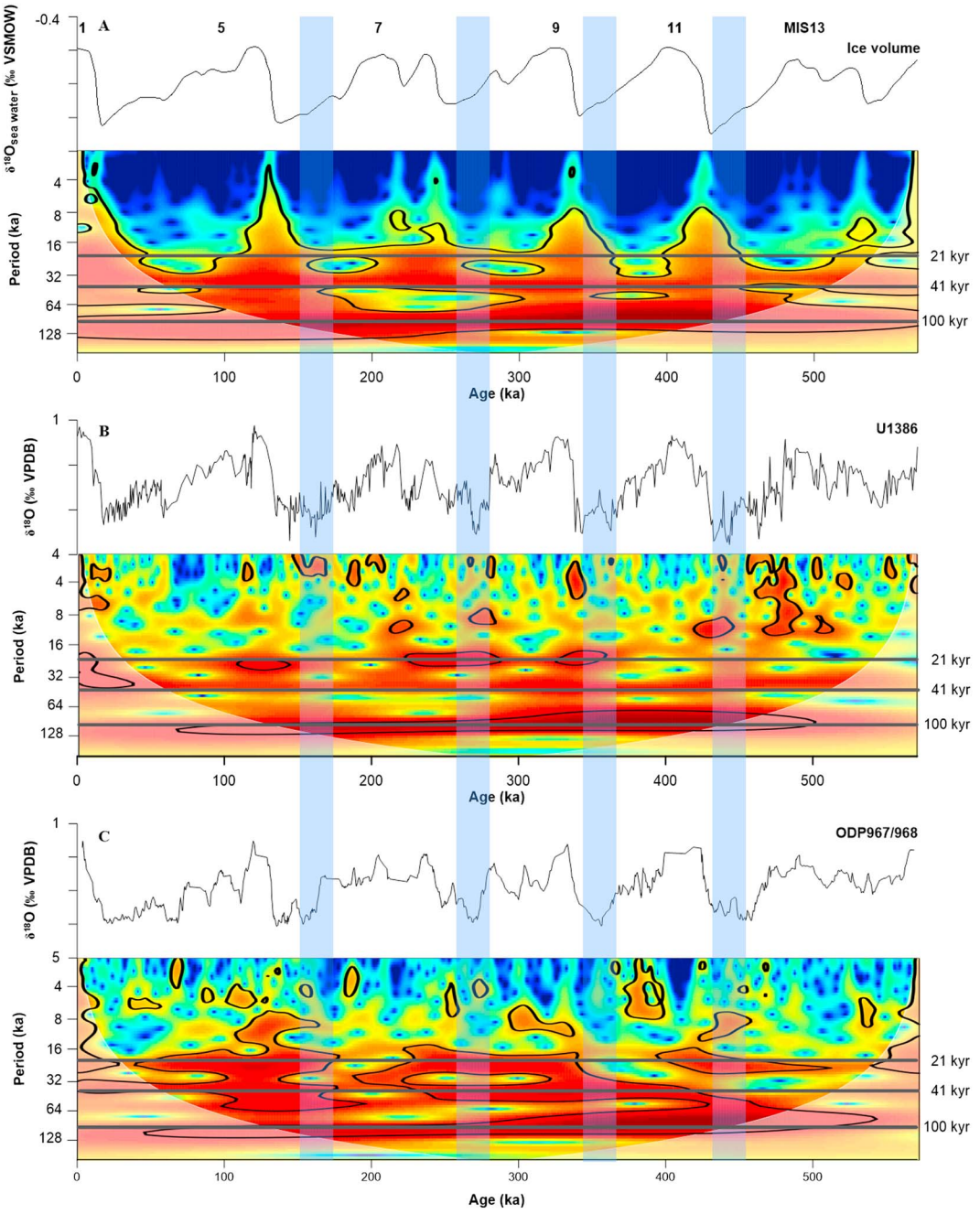

Figure 7. Wavelet analysis; occurrence of $\delta^{18}O$ enrichment events during MIS 6 to MIS 12 at Site U1386 are marked by blue columns. Marine isotope stages (MIS) following *Lisiecki and Raymo* [2005]. (a) Wavelet of $\delta^{18}O_{sea\ water}$ change relative to the present day (ice volume equivalent) derived from the benthic global $\delta^{18}O$ record LR04 [*de Boer et al.*, 2014]; (b) wavelet of benthic $\delta^{18}O$ record at Site U1386 (this study); and (c) wavelet of benthic $\delta^{18}O$ record at Sites ODP 967/968 [*Konijnendijk et al.*, 2014].

related to higher sea level than compared to the LGM but in association also to a smaller glacial reduction in deep-water temperature [*de Boer et al.*, 2014]. This indicates that a substantial part of the relative $\delta^{18}O$ discrepancy between Site U1386 and LR04 derives from the fact that the LR04 represents global mean deep-water temperature conditions which do not match the pattern of glacial temperature decrease we observe at Site U1386.

An alternative explanation for the strong precession cyclicity and the occurrence of these glacial $\delta^{18}O$ enrichment events might also be seen in the influence of subtropical water in the Gulf of Cadiz during glacials. In this scenario, the associated sea level drawdown would move the core location upward into the direction of the overlying NACW (see Figure 2). Hence, a significant part of the recorded $\delta^{18}O$ signal during these enrichment events could also relate to an increased salinity of the subtropical water masses [*Schmidt et al.*, 2006] and not to MOW influence. Initially, it was suggested that the prevalence of subtropical intermediate and surface water masses along the Iberian Margin and in extension the Gulf of Cadiz is predominately glacioeustatic driven [*Rogerson et al.*, 2004; *Voelker et al.*, 2009; *Voelker and de Abreu*, 2011]. However, recent suggestions made by *Amore et al.* [2012] for the Iberian Margin indicate a precession related migration pattern superimposed on glacial-interglacial variability. The authors argued that northward increase of subtropical waters are caused by prolonged negative North Atlantic Oscillation (NAO)-like conditions coinciding with precession maximum (LGM coincides with precession maximum at 20 ka). In this case, the weaker Azores high-Icelandic low pressure system is shifted southward, due to the decreased warming in the Northern Hemisphere in response to insolation as well as emergence of a circumpolar high-pressure belt. As a consequence of the decreased pressure gradient, the equatorward wind stress decreases aiding the northward expansion of subtropical water masses [*Moreno*, 2002; *Yin et al.*, 2009].

Independent of the forcing mechanisms, our records indicate profound changes in the characteristics of the MOW (i.e., flow speed, salinity, and temperature) over the course of the past 570 kyr. Especially, salinity increases as inferred for the glacial $\delta^{18}O$ excursion will enhance the salinity budget of the intermediate North Atlantic and stabilized or even help to invigorate the glacial overturning circulation.

6. Conclusions

The isotopic and grain size records at Site U1386 represents the first available long-term records of MOW variability and interconnected eastern North Atlantic Central Water variability from the Gulf of Cadiz during the Late and Middle Pleistocene.

We find three distinct phases of MOW variability: during Phase I (last climatic cycle) MOW influence is strengthened predominately during interglacial periods and sea level highstands whereas it is reduced or absent during glacial periods of MIS 2 and MIS 4. During Phase II (~475 to ~130 ka), MOW flow strength is generally low, though prevailed at Site U1386, and largely unaffected by the prevalent glacial-interglacial-related climatic background conditions. During Phase III (~475 to ~570 ka) MOW influence at Site U1386 is generally strengthened and persistent during MIS 14. The driving mechanism of the overall pattern of MOW variability through these three phases might relate to a distinct shift in the relative contributions of eastern Mediterranean intermediate water (Phase II) versus WMDW (Phases I and III).

Keeping pace with the change in MOW sourcing is the occurrence of distinct and precession paced $\delta^{18}O$ enrichment events contrasting the pattern of glacial behavior depicted in the global mean $\delta^{18}O$ signal (LR04). These $\delta^{18}O$ enrichment events most likely reflect a combination of (1) profound temperature reduction and salinity increases of the MOW, since it aligns with similar changes in the Mediterranean source region, (2) potentially increased ice volume, since these events are accompanied by significant sea level drops as reconstructed from Red Sea sediments, and (3) the increased influence of North Atlantic intermediate water masses when MOW influence is highly reduced or even absent at Site U1386.

Acknowledgments

First, we would like to thank two anonymous reviewers and Associate Editor Min-Te Chen for their careful handling of the manuscript as well as for their constructive comments and suggestions to improve our manuscript. We acknowledge the Integrated Ocean Drilling Program (IODP) for providing the samples used in this study as well as A. van Dijk at Utrecht University and J. Nicolson at Cambridge University for analytical support. This research was funded by NWO-ALW grant (project 865.10.001) to Lucas J. Lourens. B. de Boer receives funding from the European Union's Horizon 2020 research and innovation program under the Marie Sklodowska-Curie grant agreement 660814. All data presented in this study are available online via www.pangea.de.

References

Ambar, I., and M. R. Howe (1979), Observations of the Mediterranean outflow: II. The deep circulation in the vicinity of the Gof Cadiz, *Deep Sea Res., Part A*, doi:10.1016/0198-0149(79)90096-7.

Amore, F. O., J. A. Flores, A. H. L. Voelker, S. M. Lebreiro, E. Palumbo, and F. J. Sierro (2012), A Middle Pleistocene Northeast Atlantic coccolithophore record: Paleoclimatology and paleoproductivity aspects, *Mar. Micropaleontol.*, *90–91*, 44–59, doi:10.1016/j.marmicro.2012.03.006.

Bahr, A., et al. (2014), Deciphering bottom current velocity and paleoclimate signals from contourite deposits in the Gulf of Cadiz during the last 140 kyr: An inorganic geochemical approach: Geochemistry, *Geophysics, Geosystems*, *15*, 3145–3160, doi:10.1002/2014GC005356.

Bahr, A., et al. (2015), Persistent monsoonal forcing of Mediterranean Outflow Water dynamics during the late Pleistocene, *Geology*, *43*, 951–954, doi:10.1130/G37013.1.

Baringer, M.O., and J. F. Price (1997), Mixing and Spreading of the Mediterranean Outflow, *J. Phys. Oceanogr.*, *27*, 1654–1677, doi:10.1175/1520-0485(1997)027<1654:MASOTM>2.0.CO;2.

Barker, S., M. Greaves, and H. Elderfield (2003), A study of cleaning procedures used for foraminiferal Mg/Ca paleothermometry, *Geochem. Geophys. Geosyst.*, *4*(9), 8407, doi:10.1029/2003GC000559.

Borenäs, K. M., A. K. Wåhlin, I. Ambar, and N. Serra (2002), The Mediterranean outflow splitting—a comparison between theoretical models and CANIGO data, *Deep Sea Res., Part II*, *49*, 4195–4205, doi:10.1016/S0967-0645(02)00150-9.

Bosmans, J. H. C., S. S. Drijfhout, E. Tuenter, F. J. Hilgen, and L. J. Lourens (2014), Response of the North African summer monsoon to precession and obliquity forcings in the EC-Earth GCM, *Clim. Dyn.*, *44*, 279–297, doi:10.1007/s00382-014-2260-z.

Bryan, S. P., and T. M. Marchitto (2008), Mg/Ca-temperature proxy in benthic foraminifera: New calibrations from the Florida Straits and a hypothesis regarding Mg/Li, *Paleoceanography*, *23*, PA2220, doi:10.1029/2007PA001553.

Bryden, H. L., and H. M. Stommel (1984), Liminting processes thatdetermine basic features of the circulation in the Mediterranean Sea, *Oceanol. Acta*, *7*, 289–296.

Bryden, H. L., J. Candela, and T. H. Kinder (1994), Exchange through the Strait of Gibraltar, *Prog. Oceanogr.*, doi:10.1016/0079-6611(94)90028-0.

Cacho, I., N. Shackleton, H. Elderfield, F. J. Sierro, and J. O. Grimalt (2006), Glacial rapid variability in deep-water temperature and $\delta^{18}O$ from the Western Mediterranean Sea, *Quat. Sci. Rev.*, *25*, 3294–3311, doi:10.1016/j.quascirev.2006.10.004.

Cramp, A., and G. OSullivan (1999), Neogene sapropels in the Mediterranean: A review, *Mar. Geol.*, *153*, 11–28, doi:10.1016/S0025-3227(98)00092-9.

de Boer, B., L. J. Lourens, and R. S. W. van deWal (2014), Persistent 400,000-year variability of Antarctic ice volume and the carbon cycle is revealed throughout the Plio-Pleistocene, *Nat. Commun.*, *5*, doi:10.1038/ncomms3999.

Elderfield, H., P. Ferretti, M. Greaves, S. Crowhurst, I. N. McCave, D. Hodell, and A. M. Piotrowski (2012), Evolution of ocean temperature and ice volume through the Mid-Pleistocene climate transition, *Science*, *337*, 704–709, doi:10.1126/science.1221294.

Ferguson, J. E., G. M. Henderson, M. Kucera, and R. E. M. Rickaby (2008), Systematic change of foraminiferal Mg/Ca ratios across a strong salinity gradient, *Earth Planet. Sci. Lett.*, *265*, 153–166, doi:10.1016/j.epsl.2007.10.011.

Fiúza, A. F. G., M. Hamann, I. Ambar, G. Díaz del Río, N. González, and J. M. Cabanas (1998), Water masses and their circulation off western Iberia during May 1993, *Deep Sea Res., Part I*, *45*, 1127–1160, doi:10.1016/S0967-0637(98)00008-9.

Gouhier, T.C., A. Grinstead, and V. Simko (2016), Biwavelet: Conduct univariate and bivariate wavelet analyses (version 0.20.10).

Grant, K. M., et al. (2014), Sea-level variability over five glacial cycles, *Nat. Commun.*, *5*, 5076, doi:10.1038/ncomms6076.

Grinsted, A., J. C. Moore, and S. Jevrejeva (2004), Application of the cross wavelet transform and wavelet coherence to geophysical time series, *Nonlinear Processes Geophys.*, *11*, 561–566, doi:10.5194/npg-11-561-2004.

Hernández-Molina, F. J., et al. (2006), The contourite depositional system of the Gulf of Cádiz: A sedimentary model related to the bottom current activity of the Mediterranean outflow water and its interaction with the continental margin, *Deep Sea Res., Part II*, *53*, 1420–1463, doi:10.1016/j.dsr2.2006.04.016.

Hernández-Molina, F. J., et al. (2013), IODP Expedition 339 in the Gulf of Cadiz and off West Iberia: Decoding the environmental significance of the Mediterranean outflow water and its global influence, *Sci. Drill.*, *16*, 1–11, doi:10.5194/sd-16-1-2013.

Hernandez-Molina, F. J., et al. (2014), Onset of Mediterranean outflow into the North Atlantic, *Science*, *344*, 1244–1250, doi:10.1126/science.1251306.

Hernanndez-Molina, F. J., et al. (2015), Evolution of the Gulf of Cadiz margin and southwest Portugal contourite depositional system: Tectonic, sedimentary and paleoceanographic implications from IODP Expedition 339, *Mar. Geol.*, *377*, 7–39, doi:10.1016/j.margeo.2015.09.013.

Jiménez-Espejo, F. J., M. Pardos-Gené, F. Martínez-Ruiz, A. García-Alix, T. van deFlierdt, T. Toyofuku, A. Bahr, and K. Kreissig (2015), Geochemical evidence for intermediate water circulation in the westernmost Mediterranean over the last 20kyrBP and its impact on the Mediterranean outflow, *Global Planet. Change*, *135*, 38–46, doi:10.1016/j.gloplacha.2015.10.001.

Kaboth, S., A. Bahr, G.-J. Reichart, B. Jacobs, and L. J. Lourens (2016), New insights into upper MOW variability over the last 150kyr from IODP 339 Site U1386 in the Gulf of Cadiz, *Mar. Geol.*, *377*, 136–145, doi:10.1016/j.margeo.2015.08.014.

Köhler, P., R. Bintanja, H. Fischer, F. Joos, R. Knutti, G. Lohmann, and V. Masson-Delmotte (2010), What caused Earth's temperature variations during the last 800,000 years? Data-based evidence on radiative forcing and constraints on climate sensitivity, *Quat. Sci. Rev.*, *29*, 129–145, doi:10.1016/j.quascirev.2009.09.026.

Konijnendijk, T. Y. M., M. Ziegler, and L. J. Lourens (2014), Chronological constraints on Pleistocene sapropel depositions from high-resolution geochemical records of ODP Sites 967 and 968, *Newsl. Stratigr.*, *47*, 263–282, doi:10.1127/0078-0421/2014/0047.

Konijnendijk, T. Y. M., M. Ziegler, and L. J. Lourens (2015), On the timing and forcing mechanisms of late Pleistocene glacial terminations: Insights from a new high-resolution benthic stable oxygen isotope record of the eastern Mediterranean, *Quat. Sci. Rev.*, *129*, 308–320, doi:10.1016/j.quascirev.2015.10.005.

Lisiecki, L. E., and M. E. Raymo (2005), A Pliocene-Pleistocene stack of 57 globally distributed benthic $\delta^{18}O$ records, *Paleoceanography*, *20*, PA1003, doi:10.1029/2004PA001071.

Liu, Y., X. San Liang, and R. H. Weisberg (2007), Rectification of the bias in the wavelet power spectrum, *J. Atmos. Ocean. Technol.*, *24*, 2093–2102, doi:10.1175/2007JTECHO511.1.

Llave, E., J. Schönfeld, F. J. Hernández-Molina, T. Mulder, L. Somoza, V. Díaz Del Río, and I. Sánchez-Almazo (2006), High-resolution stratigraphy of the Mediterranean outflow contourite system in the Gulf of Cadiz during the late Pleistocene: The impact of Heinrich events, *Mar. Geol.*, *227*, 241–262, doi:10.1016/j.margeo.2005.11.015.

Llave, E., F. J. Hernández-Molina, D. A. V. Stow, M. C. Fernández-Puga, M. García, J. T. Vázquez, A. Maestro, L. Somoza, and V. Díaz del Río (2007), Reconstructions of the Mediterranean Outflow Water during the quaternary based on the study of changes in buried mounded drift stacking pattern in the Gulf of Cadiz, *Mar. Geophys. Res.*, *28*, 379–394, doi:10.1007/s11001-007-9040-7.

Meyers, S. R. (2014), Astrochron: An R package for astrochronology.

Millot, C. (2009), Another description of the Mediterranean Sea outflow, *Prog. Oceanogr.*, *82*, 101–124, doi:10.1016/j.pocean.2009.04.016.

Millot, C. (2014), Heterogeneities of in- and out-flows in the Mediterranean Sea, *Prog. Oceanogr.*, *120*, 254–278, doi:10.1016/j.pocean.2013.09.007.

Millot, C., J. Candela, J.-L. Fuda, and Y. Tber (2006), Large warming and salinification of the Mediterranean outflow due to changes in its composition, *Deep Sea Res., Part I*, *53*, 656–666, doi:10.1016/j.dsr.2005.12.017.

Moreno, A. (2002), Saharan dust transport and high-latitude glacial climatic variability: The Alboran Sea record, *Quat. Res.*, *58*, 318–328, doi:10.1006/qres.2002.2383.

Peliz, Á., J. Dubert, A. M. P. Santos, P. B. Oliveira, and B. LeCann (2005), Winter upper ocean circulation in the Western Iberian Basin—Fronts, eddies and Poleward flows: An overview, *Deep Sea Res., Part I*, *52*, 621–646, doi:10.1016/j.dsr.2004.11.005.

Peliz, A., P. Marchesiello, A. M. P. Santos, J. Dubert, A. Teles-Machado, M. Marta-Almeida, and B. LeCann (2009), Surface circulation in the Gulf of Cadiz: 2. Inflow-outflow coupling and the Gulf of Cadiz slope current, *J. Geophys. Res.*, *114*, C03011, doi:10.1029/2008JC004771.

R Core Team (2014), R: A language and environment for statistical computing.
Rahim, K. J., W. Burr, and D. J. Thomson (2014), Applications of Multitaper Spectral Analysis to Nonstationary Data - Appendix A, pp. 149–183. [Available at http://hdl.handle.net/1974/12584.]
Rogerson, M., E. J. Rohling, P. P. E. Weaver, and J. W. Murray (2004), The Azores Front since the last glacial maximum, *Earth Planet. Sci. Lett.*, *222*, 779–789, doi:10.1016/j.epsl.2004.03.039.
Rogerson, M., E. J. Rohling, P. P. E. Weaver, and J. W. Murray (2005), Glacial to interglacial changes in the settling depth of the Mediterranean Outflow plume, *Paleoceanography*, *20*, PA3007, doi:10.1029/2004PA001106.
Rogerson, M., E. J. Rohling, G. R. Bigg, and J. Ramirez (2012), Paleoceanography of the Atlantic-Mediterranean exchange: Overview and first quantitative assessment of climatic forcing, *Rev. Geophys.*, *50*, RG2003, doi:10.1029/2011RG000376.
Rohling, E. J., K. Grant, M. Bolshaw, A. P. Roberts, M. Siddall, C. Hemleben, and M. Kucera (2009), Antarctic temperature and global sea level closely coupled over the past five glacial cycles, *Nat. Geosci.*, *2*, 500–504, doi:10.1038/ngeo557.
Rossignol-Strick, M. (1985), Mediterranean Quaternary sapropels, an immediate response of the African monsoon to variation of insolation, *Palaeogeogr. Palaeoclimatol. Palaeoecol.*, *49*, 237–263, doi:10.1016/0031-0182(85)90056-2.
Schmidt, M. W., M. J. Vautravers, and H. J. Spero (2006), Rapid subtropical North Atlantic salinity oscillations across Dansgaard-Oeschger cycles, *Nature*, *443*, 561–564, doi:10.1038/nature05121.
Schönfeld, J. (2002), A new benthic foraminiferal proxy for near-bottom current velocities in the Gulf of Cadiz, northeastern Atlantic Ocean, *Deep Sea Res., Part I*, *49*, 1853–1875, doi:10.1016/S0967-0637(02)00088-2.
Schönfeld, J., and R. Zahn (2000), Late Glacial to Holocene history of the Mediterranean outflow. Evidence from benthic foraminiferal assemblages and stable isotopes at the Portuguese margin, *Palaeogeogr. Palaeoclimatol. Palaeoecol.*, *159*, 85–111, doi:10.1016/S0031-0182(00)00035-3.
Shackleton, N. J., and M. B. Cita (1979), Oxygen and carbon isotope stratigraphy of benthic foraminifers at site 397: Detailed history of climatic change during the Late Neogene, U.S. Gov. Print. Office.
Shackleton, N. J., and M. A. Hall (1984), Oxygen and carbon isotope stratigraphy of the deep sea drilling project hole 552A: Plio-Pleistocene glacial history, *Initial Rep. DSDP*, *81*, 599–609.
Siddall, M. (2004), Understanding the Red Sea response to sea level, *Earth Planet. Sci. Lett.*, *225*, 421–434, doi:10.1016/j.epsl.2004.06.008.
Stevenson, R. E. (1977), Huelva Front and Malaga, Spain, eddy chain as defined by satellite and oceanographic data, *Dtsch. Hydrogr. Zeitschrift*, *30*, 51–53, doi:10.1007/BF02226082.
Stow, D.A.V., F. J. Hernández-Molina, and C. Alvarez-Zarikian (2013), Expedition 339 summary, doi:10.2204/iodp.proc.339.104.2013.
Taner, M. (1992), Attributes Revisited (Technical Report, Rock Solid).
Thomson, D. J. (1982), Spectrum estimation and harmonic analysis, *Proc. IEEE*, *70*, 1055–1096, doi:10.1109/PROC.1982.12433.
Torrence, C., and G. P. Compo (1998), A practical guide to wavelet analysis, *Bull. Am. Meteorol. Soc.*, *79*, 61–78, doi:10.1175/1520-0477(1998)079<0061:APGTWA>2.0.CO;2.
Voelker, A., S. Lebreiro, J. Schonfeld, I. Cacho, H. Erlenkeuser, and F. Abrantes (2006), Mediterranean outflow strengthening during northern hemisphere coolings: A salt source for the glacial Atlantic?, *Earth Planet. Sci. Lett.*, *245*, 39–55, doi:10.1016/j.epsl.2006.03.014.
Voelker, A. H. L., and L. de Abreu (2011), A review of abrupt climate change events, in *The Northeastern Atlantic Ocean (Iberian Margin): Latitudinal, Longitudinal, and Vertical Gradients*, edited by H. Rashid, L. Polyak, and E. Mosley-Thompson, pp. 15–37, AGU, Washington, D. C.
Voelker, A. H. L., L. de Abreu, J. Schönfeld, H. Erlenkeuser, and F. Abrantes (2009), Hydrographic conditions along the western Iberian margin during marine isotope stage 2, *Geochem. Geophys. Geosyst.*, *10*, Q12U08, doi:10.1029/2009GC002605.
Voelker, A. H. L., A. Colman, G. Olack, J. J. Waniek, and D. Hodell (2015), Oxygen and hydrogen isotope signatures of Northeast Atlantic water masses, *Deep Sea Res., Part II*, *116*, 89–106, doi:10.1016/j.dsr2.2014.11.006.
Wang, P., J. Tian, X. Cheng, C. Liu, and J. Xu (2003), Carbon reservoir changes preceded major ice-sheet expansion at the mid-Brunhes event, *Geology*, *31*, 239, doi:10.1130/0091-7613(2003)031<0239:CRCPMI>2.0.CO;2.
Wang, P., J. Tian, and L. J. Lourens (2010), Obscuring of long eccentricity cyclicity in Pleistocene oceanic carbon isotope records, *Earth Planet. Sci. Lett.*, *290*, 319–330, doi:10.1016/j.epsl.2009.12.028.
Yin, Q. Z., A. Berger, and M. Crucifix (2009), Individual and combined effects of ice sheets and precession on MIS-13 climate, *Clim. Past*, *5*, 229–243, doi:10.5194/cp-5-229-2009.
Zahn, R., M. Sarnthein, and H. Erlenkeuser (1987), Benthic isotope evidence for changes of the Mediterranean outflow during the Late Quaternary, *Paleoceanography*, *2*, 543–559, doi:10.1029/PA002i006p00543.